Longitudinal Evaluation of Early Alzheimer's Disease Using Brain Perfusion SPECT

Daiji Kogure, Hiroshi Matsuda, Takashi Ohnishi, Takashi Asada, Masatake Uno, Toshiyuki Kunihiro, Seigo Nakano, and Masaru Takasaki

Departments of Radiology, Psychiatry, and Geriatric Medicine, National Center Hospital for Mental, Nervous, and Muscular Disorders, National Center of Neurology and Psychiatry, Tokyo; and Department of Geriatric Medicine, Tokyo Medical University, Tokyo, Japan

The aim of this SPECT study was to determine the initial abnormality and longitudinal changes in regional cerebral blood flow (rCBF) in early Alzheimer's disease (AD) using statistical parametric mapping (SPM). **Methods:** rCBF was noninvasively measured using ^{99m}Tc-ethyl cysteinate dimer SPECT in 32 patients complaining of mild cognitive impairment, with a Mini-Mental State Examination score more than 24 at the initial study, and 45 age-matched healthy volunteers. All patients satisfied the diagnostic criteria of AD during the follow-up period of at least 2 y. Follow-up SPECT studies were performed on the patients at a mean interval of 15 mo. We used the raw data (absolute rCBF parametric maps) and the adjusted rCBF images of relative flow distribution (normalization of global cerebral blood flow [CBF] for each subject to 50 mL/100 g/min with proportional scaling) to compare these groups with SPM. **Results:** In the baseline study, the adjusted rCBF was significantly and bilaterally decreased in the posterior cingulate gyri and precunei of patients compared with healthy volunteers. In the follow-up study, selected reduction of the adjusted rCBF was observed in the left hippocampus and parahippocampal gyrus. These areas showed the most prominent reduction in absolute rCBF on each occasion. Moreover, further decline of the absolute rCBF was longitudinally observed in extensive areas of the cerebral association cortex. **Conclusion:** SPM analysis showed the characteristic early-AD rCBF pattern of selective decrease and longitudinal decline, which may be overlooked by a conventional region-of-interest technique with observer a priori choice and hypothesis. This alteration in rCBF may closely relate to the pathophysiologic process of this disease.

Key Words: Alzheimer's disease; SPECT; regional cerebral blood flow; statistical parametric mapping

J Nucl Med 2000; 41:1155–1162

In the investigation of Alzheimer's disease (AD), recent in vivo neuroimaging developments have allowed MRI, PET, and SPECT to reveal volume decreases for medial temporal structures and reductions in regional cerebral blood flow (rCBF) in temporoparietal areas (*1–4*). However, few longitudinal studies have examined the imaging characteristics of early AD.

Most imaging studies of AD have been analyzed by a region-of-interest (ROI) technique. Although this approach has gained general acceptance, it is limited by the fact that the selection of sample depends on the observer's a priori choice and hypothesis and leaves large areas of the brain unexplored. An alternative method is voxel-by-voxel analysis in stereotactic space to avoid subjectivity and to adopt the principle of data-driven analysis. Such an approach is well established in the field of functional neuroimaging analysis. A software package known as statistical parametric mapping (SPM) has been developed that not only spatially normalizes PET or SPECT images to a standardized stereotactic space but then also statistically analyzes groups of images (*5*). We performed this study to evaluate the progression of rCBF abnormalities over time in early AD by application of SPM to brain perfusion SPECT images.

MATERIALS AND METHODS

Subjects

Thirty-two patients (13 men, 19 women; age range, 54–84 y; mean age, 72.1 y) who complained of only memory impairment were recruited from an outpatient memory clinic of the National Center Hospital for Mental, Nervous, and Muscular Disorders, National Center of Neurology and Psychiatry, between 1995 and 1997. The recruitment was for an ongoing study of AD. The clinical diagnosis of AD was based on the fourth edition of the *Diagnostic and Statistical Manual of Mental Disorders* (*DSM-IV*) (*6*) and on the criteria of the National Institute of Neurological and Communicative Disorders and Stroke and the Alzheimer's Disease and Related Disorders Association (*7*). For all patients, the evaluated stage of dementia corresponded to 0.5 in the clinical dementia rating (*8*). All patients underwent thorough neuropsychologic testing that revealed quantified, objective evidence of memory impairment with no apparent loss in general cognitive, behavioral, or functional status at the initial study. The classification of memory impairment required normal mental status with a score of more than 24 on the Mini-Mental State Examination (MMSE). As shown in Table 1, the memory performance of all patients was significantly impaired, seen most prominently through verbal and nonverbal episodic memory tests comprising digit span, learning of

Received Jul. 6, 1999; revision accepted Nov. 1, 1999.

For correspondence or reprints contact: Hiroshi Matsuda, MD, Department of Radiology, National Center Hospital for Mental, Nervous, and Muscular Disorders, National Center of Neurology and Psychiatry, 4-1-1, Ogawahigashi, Kodaira, Tokyo, 187-8551, Japan.

TABLE 1
Mean Performance Levels in Neuropsychological Assessment

Subject	MMSE	Digit span		Word learning (10 words) delayed recall (30 min)	Story recall (15 elements)		Rey-Osterrieth complex figure test		
		Forward	Backward		Immediate	Delayed (30 min)	Copy	Recall: Immediate	Recall: Delayed (30 min)
Healthy volunteers	28.3 ± 1.7	5.3 ± 0.6	4.2 ± 0.7	8.0 ± 1.0	9.6 ± 3.6	8.0 ± 2.7	35.6 ± 0.8	19.9 ± 4.3	18.8 ± 5.6
Early AD patients									
Baseline	26.2 ± 1.5	5.3 ± 0.8	3.8 ± 0.8	1.4 ± 2.3*	4.7 ± 2.4*	0.7 ± 1.5*	33.2 ± 4.7	7.0 ± 4.6*	4.8 ± 4.8*
Follow-up	22.3 ± 3.6*	5.2 ± 0.9	3.7 ± 0.8	1.2 ± 2.4*	4.3 ± 2.4*	1.5 ± 1.3*	32.6 ± 5.1	6.4 ± 5.0*	4.0 ± 4.9*

*Mean differs from healthy volunteers, $P < 0.001$.
†Mean differs from baseline, $P < 0.001$.
Values are mean ± SD.

a list of 10 words, story recall, and the Rey-Osterrieth complex figure test (*9*). Selective impairment of delayed recall is the most prominent neuropsychologic feature of patients with an early stage of AD (*10*). Each patient underwent baseline SPECT and MRI at the time of the initial evaluation, was followed up clinically, and underwent a second SPECT examination at intervals ranging from 11 to 25 mo (mean, 15 mo). At the time of the baseline SPECT study, the MMSE score was 26.2 ± 1.5 (mean ± SD); this mean declined to 22.3 ± 3.6 at the time of the follow-up SPECT study. The MMSE score showed a further decline to 20.8 ± 5.1 during subsequent clinical follow-up for at least 2 y. Nineteen patients (59%) showed an MMSE score of less than 24 at the follow-up SPECT study, and 24 patients (75%) showed scores of less than 24 during further clinical follow-up. At the time of study entry, none of the 32 patients met AD criteria according to DSM-IV. However, during the observation period, the patients showed a progressive cognitive decline and eventually fulfilled the AD criteria. No focal brain lesions on MRI were observed except for age-related white matter hyperintensities on T2-weighted images.

Forty-five healthy volunteers (14 men, 31 women; age range, 54–87 y; mean age, 68.2 y) were also studied. They had no neurologic or psychiatric disorders, including alcoholism, substance abuse, atypical headache, head trauma with consciousness loss, and asymptomatic cerebral infarction detected by T2-weighted MRI. They did not significantly differ in age, sex, or educational level from the AD patients. The ethics committee of the National Center of Neurology and Psychiatry approved this study for healthy volunteers, all of whom gave informed consent to participate.

Global and rCBF Measurements

Before SPECT was performed, an intravenous line was established in all subjects. They were injected while lying down with eyes closed. Each received a 600-MBq intravenous injection of ^{99m}Tc-ethyl cysteinate dimer. The global CBF was noninvasively measured using graphic analysis, as has been described in reports without any blood sampling (*11,12*). The passage of the tracer from the aortic arch to the brain was monitored in a 128 × 128 format for 100 s at 1-s intervals using a rectangular gamma camera with a parallel-hole collimator on a triple-head SPECT system (Multispect3; Siemens Medical Systems, Inc., Hoffman Estates, IL). ROIs were drawn by hand over the aortic arch (ROI_{aorta}) and both brain hemispheres (ROI_{brain}). A hemispheric brain perfusion index (BPI) was determined as follows before the start of initial backdiffusion of the tracer from brain to blood (*11*):

$$BPI = 100 \times ku \frac{10 \times ROI_{aorta}size}{ROI_{brain}size}, \quad \text{Eq. 1}$$

where ku is the unidirectional influx rate for the tracer from blood to brain, which is determined by the slope of the line in graphic analysis within the first 30 s after injection. Then, the BPI (x) was converted to global cerebral blood flow (CBF) values (y) using a regression equation ($y = 2.60x + 19.8$) obtained from previous ^{133}Xe inhalation studies (*11*).

Ten minutes after the injection of ^{99m}Tc-ethyl cysteinate dimer, brain SPECT was performed using a camera equipped with high-resolution fanbeam collimators. For each camera, projection data were obtained in a 128 × 128 format for 24 angles of 120° at 50 s per angle. A Shepp and Logan Hanning filter was used for SPECT image reconstruction at 0.75 cycle/cm. Attenuation correction was performed using Chang's method. To calculate rCBF and to correct for incomplete retention of ^{99m}Tc-ethyl cysteinate dimer in the brain, the following linearization algorithm (*13*) of a curvilinear relationship between brain activity and blood flow was applied:

$$Fi = Fr \times \frac{\alpha \times (Ci/Cr)}{[1 + \alpha - (Ci/Cr)]}, \quad \text{Eq. 2}$$

where Fi and Fr represent CBF values for a region i and a reference region r, respectively, and Ci and Cr are the SPECT counts for the region i and the reference region r, respectively. The cerebral hemisphere was used as the reference region, and global CBF obtained from graphic analysis was substituted for Fr. The linearization factor α was set to 2.59, as proposed by Friberg et al. (*13*).

Image Formatting

All subsequent image manipulation and data analysis were performed on a personal computer equipped with a UNIX operating system (Linux, version 4.2; Red Hat, Inc., Durham, NC) as described previously (*14*). The software for image manipulation included MATLAB, version 4.2c (MathWorks, Inc., Natick, MA) and SPM96. Transverse slice image volumes were converted to ANALYZE format (Biomedical Imaging Resources, Mayo Foundation, Rochester, MN). The images were then spatially normalized in SPM96 to a standardized stereotactic space based on the Talairach and Tournoux atlas (*15*), using 12-parameter linear affine

normalization and a further 8 nonlinear iteration algorithms with an original template for ^{99m}Tc-ethyl cysteinate dimer. This original template was generated from 60 healthy volunteers, aged 20–79 y. Then, isotropic smoothing with 12 mm full width at half maximum was performed. This resolution corresponds to almost twice that (7.6 mm full width at half maximum) of the SPECT scanner. The initial parameters of the image were 128 × 128 × n, where n = the number of slices covering the whole brain. The final image format was 16-bit, with a size of 79 × 95 × 68 mm and a voxel size of 2 × 2 × 2 mm.

Image Analysis

Data were analyzed using the SPM96 program. Statistical parametric maps are spatially extended statistical processes used to characterize regionally specific effects in imaging data. The SPM96 combines the general linear model and the theory of gaussian fields (*16,17*) to make statistical inferences about regional effects. To examine images for specific regions of differences in perfusion between the AD patients and healthy volunteers, we compared the 2 groups using 2 contrasts in statistical analysis of SPM96. The first contrast examined areas of increased perfusion in the AD group, as compared with the control group, and the second contrast examined areas of decreased perfusion. Moreover, to examine perfusion changes from baseline to follow-up studies in the AD patients, the 2 conditions were compared in a paired manner using 2 contrasts (multisubject with different conditions in SPM96). The analysis was performed with or without the implication of changes in global CBF levels as a confounding covariate. The gray matter threshold was set to 0.8. We first used the raw data (absolute rCBF parametric maps without global normalization) and then adjusted rCBF images (normalization of global CBF for each subject to 50 mL/100 g/min with proportional scaling) to compare 2 groups regarding relative rCBF distribution. The resulting set of values for each contrast constituted a statistical parametric map of the *t* statistic SPM {t}. The SPM {t} maps were then transformed to the units of normal distribution (SPM {Z}), and height threshold was set to $P = 0.001$. The resulting regions were examined with multiple comparisons. The significance of each region was estimated with a threshold of $P = 0.05$ using distributional approximations from the theory of gaussian fields (*17*). These areas of significance were best visualized as overlaid on a normalized MR image to obtain a clear view of the location of the perfusion changes.

RESULTS

Global Effects

The baseline and follow-up global CBFs of AD patients were 38.4 ± 4.6 and 37.2 ± 5.0 mL/100 g/min, respectively, without significant changes. The follow-up global CBF of AD patients was significantly lower ($P < 0.001$) than that of healthy volunteers, at 42.1 ± 4.3 mL/100 g/min in Tukey-Kramer as a posthoc 1-way ANOVA test in the statistical software program JMP, version 3.1 (SAS Institute, Cary, NC).

Regional Effects

Absolute rCBF. Figure 1 shows the voxels with a significant decline in absolute rCBF in AD patients compared with

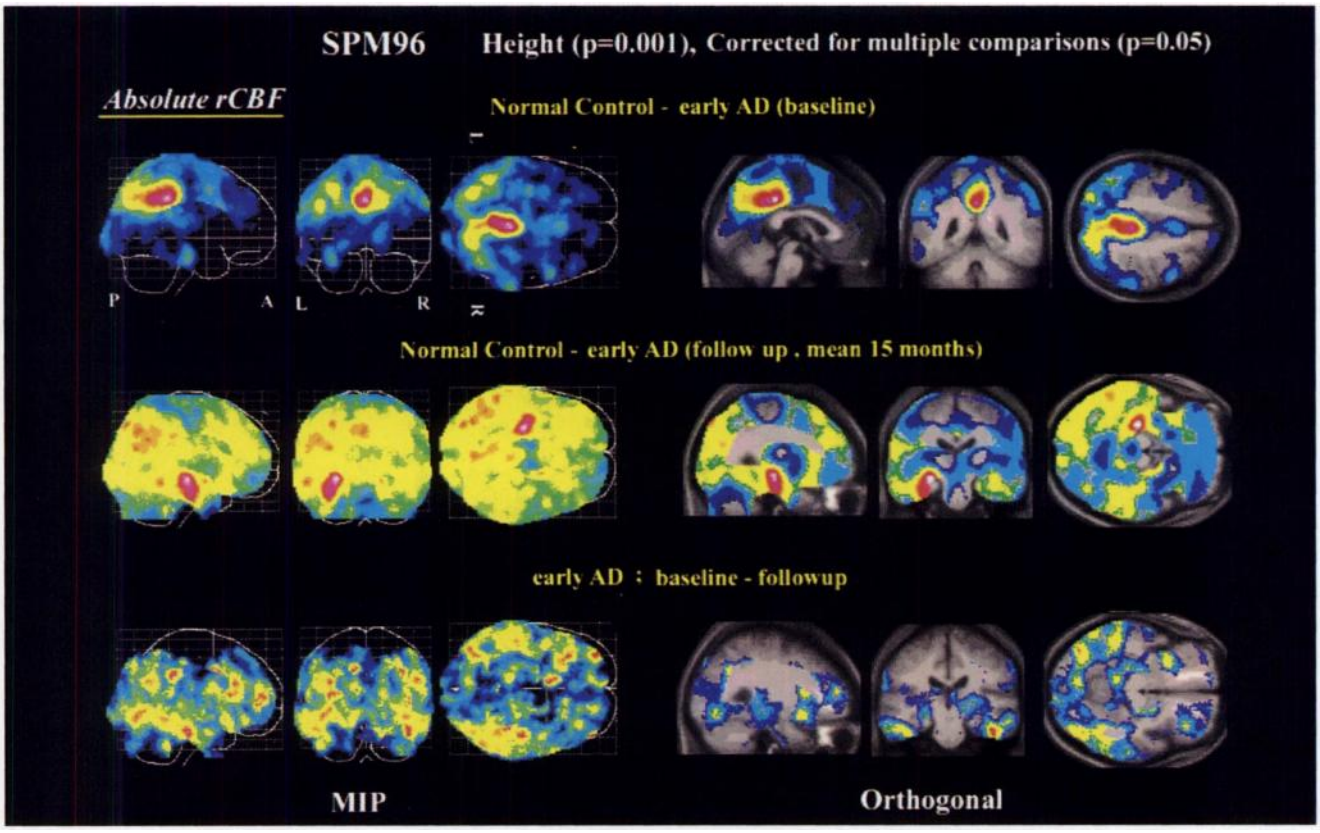

FIGURE 1. Absolute rCBF decrease shown by SPM in patients with early AD compared with healthy volunteers and from baseline to follow-up study. Significant decrease is shown as maximum-intensity projection (MIP) and colored areas superimposed on orthogonal sections of standard MR scans.

healthy volunteers and from the baseline to the follow-up study (no voxel significantly increased). A significant rCBF reduction was observed in both posterior cingulate gyri, both precunei, both parietal lobules, and the left angular and superior occipital gyri of AD patients in the baseline study compared with healthy volunteers. In the follow-up study, the left hippocampus, left fusiform gyrus, right amygdaloid body, and both temporal lobules became additionally involved. Follow-up studies showed a significant rCBF decline from the baseline study in both middle frontal gyri, both inferior temporal gyri, the left middle and inferior occipital gyri, the right inferior parietal lobules, and the left hippocampus. Table 2 lists the peaks of the most significant declines in absolute rCBF obtained in this analysis with Talairach and Tournoux coordinates (*15*), x, y, and z in millimeters of these peaks, as well as the corresponding *z* scores.

Adjusted rCBF. Figure 2 and Table 3 show the voxels with a significant decline in adjusted rCBF compared with healthy volunteers and from the baseline to the follow-up study. A significant, bilateral rCBF reduction was observed in the posterior cingulate gyri and precunei of AD patients in the baseline study compared with the healthy volunteers. In the follow-up study, the left hippocampus and left parahippocampal gyrus showed significant reductions. Follow-up studies also showed significant declines from the baseline study in the left hippocampus and left parahippocampal gyrus.

Figure 3 and Table 4 show the voxels with a significant increase in adjusted rCBF in AD patients compared with healthy volunteers and from the baseline to the follow-up study. A significant rCBF increase was observed in the left thalamus, left putamen, and right insula of AD patients in the baseline study compared with healthy volunteers. In the follow-up study, the pons, both putamina, both cerebellar hemispheres, both precentral gyri, and the right posterior central gyrus showed significant increases. Follow-up studies showed significant increases from the baseline study in the lobulus paracentralis, both postcentral gyri, the right cerebellar hemisphere, the right precuneus, the right superior frontal gyrus, the right posterior cingulate gyrus, the pons, the right putamen, and the right cuneus.

DISCUSSION

Recent PET studies have revealed selective rCBF decreases in the posterior cingulate gyrus and precuneus not only in mild to moderate AD but also in very early AD using a stereotactic anatomic standardization technique such as SPM (*18–21*). These reductions remained significant even after correction of partial-volume effects using segmented MR images (*21*). We showed the same finding in the initial baseline SPECT study. In the recent SPM analysis of AD of

TABLE 2
Location and Peaks of Significant Decreases in Absolute rCBF

Study	Structure	Coordinates			*z* score
		x	y	z	
Baseline of early AD patients versus healthy volunteers	Both posterior cingulate gyri	0	−38	38	5.75
	Left precuneus	−4	−52	36	5.61
	Right precuneus	2	−68	40	5.09
	Right inferior parietal lobules	16	−78	38	4.97
	Left superior parietal lobules	−34	−76	52	4.92
	Left angular gyrus	−46	−60	34	4.65
	Left superior occipital gyrus	−30	−84	36	4.42
Follow-up of early AD patients versus healthy volunteers	Left hippocampus	−26	−20	−12	6.73
	Left fusiform gyrus	−36	−16	−24	6.53
	Right precuneus	2	−70	38	5.99
	Left angular gyrus	−46	−60	28	5.97
	Left middle occipital gyrus	−36	−74	22	5.96
	Left inferior temporal gyrus	−58	−50	−16	5.90
	Right amygdala	20	−2	−14	5.90
	Right posterior cingulate gyrus	2	−34	32	5.84
	Left middle temporal gyrus	−54	−64	20	5.80
	Left precuneus	−10	−52	38	5.79
Follow-up versus baseline	Left middle occipital gyrus	−36	−74	−4	5.62
	Right middle frontal gyrus	48	46	6	5.57
	Left inferior occipital gyrus	−46	−78	−16	5.55
	Left middle frontal gyrus	−38	56	10	5.43
	Right inferior parietal lobules	40	−40	32	5.41
	Left hippocampus	−24	−20	−8	5.24
	Right inferior temporal gyrus	48	−26	−30	5.16
	Left inferior temporal gyrus	−46	−28	−26	5.13

Significance is at the $P < 0.001$ level.

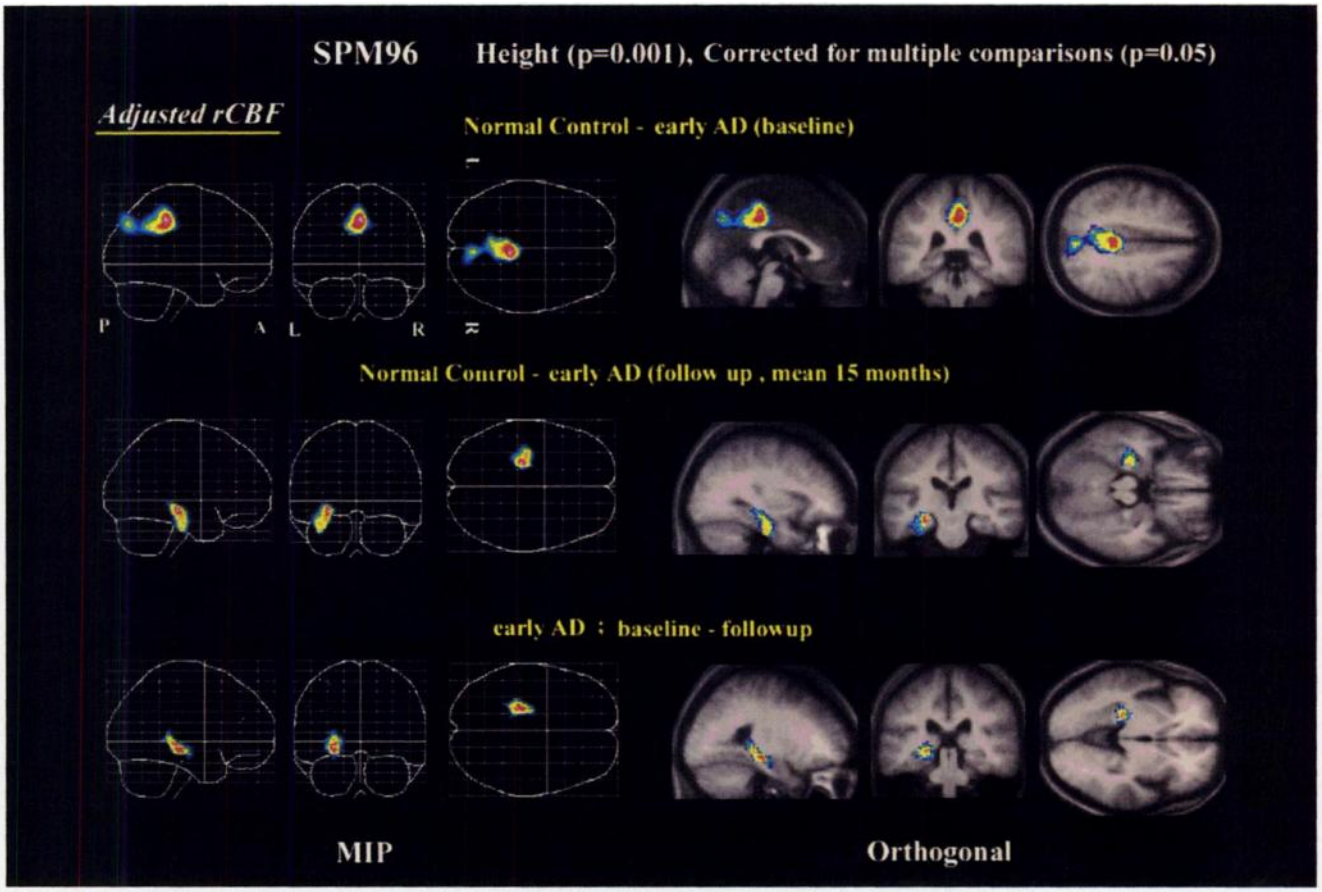

FIGURE 2. Adjusted rCBF decrease shown by SPM in patients with early AD compared with healthy volunteers and from baseline to follow-up study. MIP = maximum-intensity projection.

mild to moderate severity, a significant correlation was revealed between verbal and visual episodic memory scores and rCMRglu in the posterior cingulate gyrus (*22*). A PET activation study revealed that encoding and retrieval of episodic memory was associated with activation of the posterior cingulate gyrus and precuneus, respectively (*23*). Clinical evidence also supports the involvement of the retrosplenial cingulate cortex in the memory system (*24,25*). Although the posterior cingulate gyrus and precuneus still showed a significantly lower absolute rCBF in the follow-up study, the adjusted rCBF of AD patients did not show a significant decrease in the follow-up study compared with

TABLE 3
Location and Peaks of Significant Decreases in Adjusted rCBF

Study	Structure	Coordinates			*z* score
		x	y	z	
Baseline of early AD patients versus healthy volunteers	Right posterior cingulate gyrus	4	−34	44	5.08
	Right posterior cingulate gyrus	4	−42	38	4.61
	Left posterior cingulate gyrus	−6	−44	38	4.39
	Right precuneus	2	−70	38	4.12
	Left precuneus	−8	−52	38	4.08
Follow-up of early AD patients versus healthy volunteers	Left hippocampus	−26	−22	−12	4.87
	Left parahippocampal gyrus	−34	−18	−30	4.47
	Left parahippocampal gyrus	−28	−20	−20	4.46
Follow-up versus baseline	Left hippocampus	−24	−28	−6	4.57
	Left hippocampus	−26	−34	0	4.14
	Left hippocampus	−22	−12	−14	4.12
	Left parahippocampal gyrus	−14	−36	−2	3.18

Significance is at the $P < 0.001$ level.

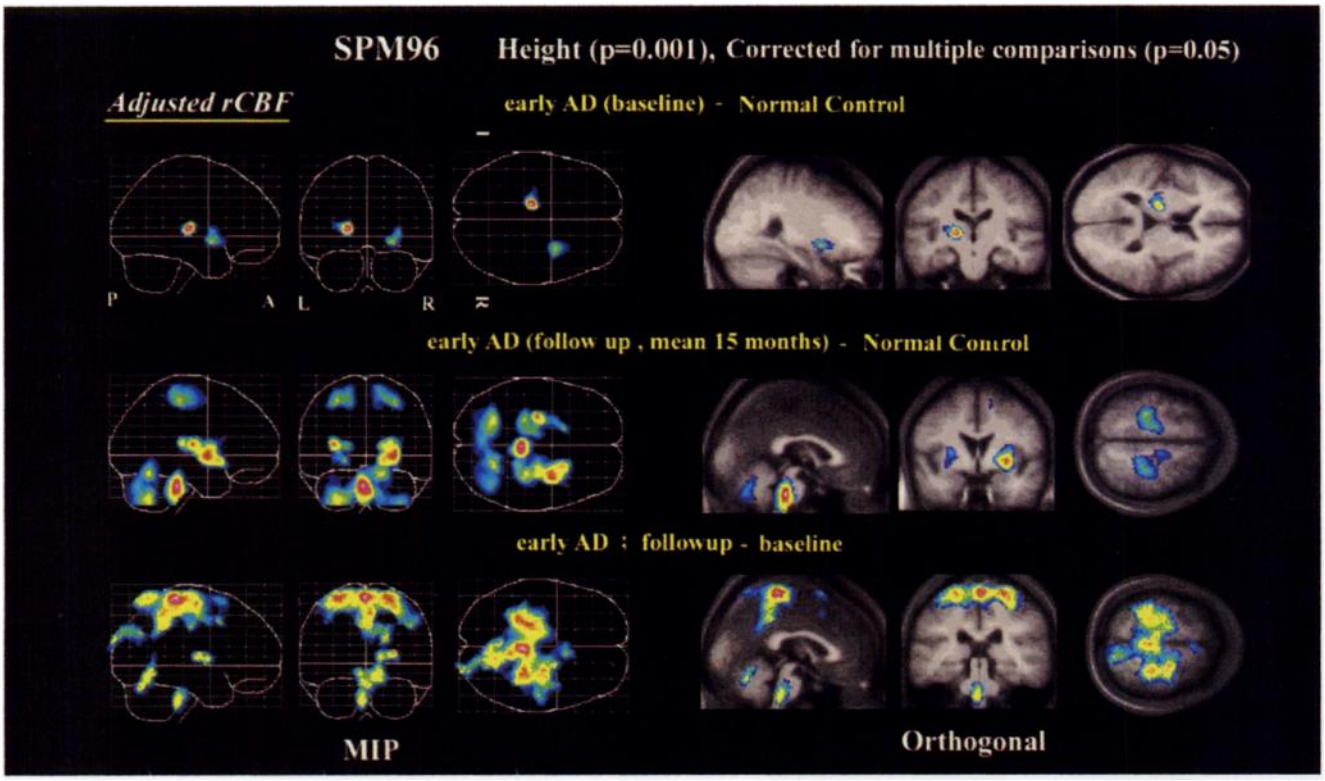

FIGURE 3. Adjusted rCBF increase shown by SPM in patients with early AD compared with healthy volunteers and from baseline to follow-up study. MIP = maximum-intensity projection.

healthy volunteers. This vanishing phenomenon of the significant decrease in adjusted rCBF from the first to the second study may be caused by considerable stability of the absolute rCBF in these areas during this period. This possibility was supported by the SPM maps of the second minus the first study with a significant increase in adjusted rCBF in these areas, which also showed well-known preserved areas in AD such as primary sensorimotor areas, cerebellum, basal ganglia, thalamus, and pons (*1,2,26*).

Most previous pathologic and morphologic studies suggest that structures within the medial temporal structures, amygdala, hippocampal formation, enthorhinal cortex, and parahippocampal and fusiform gyri are the first to be affected in AD (*4,27–30*). The reduced rCBF in the medial temporal structures shown by a recent high-resolution SPECT system is consistent with these pathologic findings (*31–33*). The current follow-up study also revealed significant reductions in the absolute and adjusted rCBF in the medial temporal area on the left side, although the possibility cannot be excluded that this decrease may be related to a partial-volume effect from focal atrophy. However, our recent cross-sectional study (*34*) on simultaneous anatomic and functional measurements using MRI and SPECT explains that the rCBF reduction in the hippocampus is not caused solely by a partial-volume effect in AD. Early AD patients showed much less decline in rCBF (12.4% on average) than in volume (22.2%) in the hippocampus compared with healthy volunteers, whereas advanced AD patients showed an almost equal decline in rCBF (25.9%) and in volume (29.3%). This much greater difference in rCBF than in volume between early and advanced AD patients is attributable not to a mere partial-volume effect but to the disease process.

Two reports (*31,32*) did not describe asymmetry in rCBF reduction in the medial temporal areas of AD, whereas Rodriguez et al. (*33*) reported that a more stringent statistical correlation exists between right hippocampal perfusion and both quantitative EEG and neuropsychologic score. Most MRI volumetric studies have shown significant asymmetry in the hippocampal volume (*4,29,35*). This discrepancy may be attributed to the greater variance of rCBF in the right hippocampus than in the left. A less stringent height threshold at $P = 0.005$ shows an additional statistical decrease in the absolute rCBF in the right hippocampus in the current follow-up study. A recent volumetric study (*36*) revealed that the right hippocampal region is smaller than the left in healthy volunteers carrying the apolipoprotein Eϵ4 allele, which is a risk factor for late-onset AD but not in those without the ϵ4 allele. AD patients with 2 ϵ4 alleles have been reported to have severe damage in the medial temporal structures early in the disease process and differ from the AD patients with 1 or no ϵ4 alleles (*37*). A further comparative SPECT study of AD patients with or without the ϵ4 alleles would clarify the rCBF variance and asymmetry in the medial temporal structures.

Several investigators have addressed longitudinal changes

TABLE 4
Location and Peaks of Significant Increases in Adjusted rCBF

Study	Structure	Coordinates			z score
		x	y	z	
Baseline of early AD patients versus healthy volunteers	Left thalamus	−16	−18	6	4.63
	Right insula	36	6	0	3.83
	Right insula	28	14	−8	3.65
	Left putamen	−26	−16	10	3.54
Follow-up of early AD patients versus healthy volunteers	Pons	0	−28	−28	5.86
	Right putamen	30	2	−2	5.55
	Left putamen	−30	−12	10	5.49
	Right putamen	20	14	−6	5.09
	Left cerebellum	−28	−56	−46	4.63
	Right cerebellum	20	−56	−20	4.55
	Right precentral gyrus	32	−26	54	4.48
	Left precentral gyrus	−26	−26	54	4.48
	Right postcentral gyrus	22	−32	56	4.30
Follow-up versus baseline	Right lobulus paracentralis	2	−32	66	4.82
	Left postcentral gyrus	−26	−32	66	4.59
	Right postcentral gyrus	28	−34	62	4.57
	Right cerebellum	4	−68	−24	4.49
	Right precuneus	6	−44	50	4.48
	Right superior frontal gyrus	24	−10	62	4.41
	Right posterior cingulate gyrus	4	−44	36	4.32
	Right precentral gyrus	32	−28	54	4.31
	Pons	0	−30	−32	4.27
	Right putamen	18	0	6	4.10
	Right cuneus	24	−88	28	4.05
	Right precuneus	8	−68	32	3.95

Significance is at the $P < 0.001$ level.

of rCBF or rCMRglu alteration in AD (*2,37–40*). However, most of the studied subjects had probable AD with MMSE scores less than 24, and cerebral association cortices were only roughly evaluated using ROI analysis. The posterior association cortex has consistently been reported to be the first cortical region affected in AD. This deficit then spreads to the frontal lobes as the disease progresses, with persisting asymmetry. In our longitudinal study, the left hippocampus and parahippocampal gyrus showed the most prominent decrease in adjusted rCBF in addition to a decline in the absolute rCBF in the cerebral association cortices. Both the high spatial resolution of the SPECT system used and the fully automated, user-independent analysis using SPM enabled us to detect rCBF changes in the fine structures of the medial temporal areas.

This study showed considerably rapid chronologic alteration of the rCBF distribution pattern in early AD. SPM analysis using both absolute and adjusted rCBF was useful for characterizing this alteration. The analysis of absolute rCBF revealed an overall tendency toward a diffuse decrease in extensive areas of the brain, and the analysis of the adjusted rCBF distinguished the regions with the most prominent decrease or increase. The reason that the rCBF decrease in the posterior cingulate gyrus and precuneus preceded that of the medial temporal areas is unclear. Functional or structural deafferentation caused by primary neural degeneration in the medial temporal areas may lead to the rCBF decrease in the posterior cingulate cortex and precuneus in the early stage of AD, as suggested by Minoshima et al. (*19*). A longitudinal combined study of functional and morphologic imaging will be necessary to further elucidate this issue.

CONCLUSION

SPM analysis showed the characteristic rCBF pattern in early AD. Initially, a selective rCBF decrease was observed in the posterior cingulate cortex and precuneus. A longitudinal rCBF decline was then observed most prominently in the left hippocampus and parahippocampal gyrus. These findings may closely relate to the pathophysiologic process of this disease. The SPM technique makes objective investigation possible and is useful for exploring regions with rCBF alteration in AD that may be overlooked by a conventional ROI technique.

ACKNOWLEDGMENTS

The authors thank the technologist staff for acquiring the data and John Gelblum for proofreading the manuscript.

REFERENCES

1. McGeer PL, Kamo H, Harrop R, et al. Comparison of PET, MRI and CT with pathology in a proven case of Alzheimer's disease. *Neurology.* 1986;36:1569–1574.

2. Duara R, Grady C, Haxby J, et al. Positron emission tomography in Alzheimer's disease. *Neurology.* 1986;36:879–887.
3. Johnson KA, Holman BL, Mueller SP, et al. Single photon emission computed tomography in Alzheimer's disease: abnormal iofetamine I 123 uptake reflects dementia severity. *Arch Neurol.* 1988;45:392–396.
4. Pearlson GD, Harris GJ, Powers RE, et al. Quantitative changes in mesial temporal volume, regional cerebral blood flow, and cognition in Alzheimer's disease. *Arch Gen Psychiatry.* 1992;49:402–408.
5. Frackowiak RSJ, Friston KJ, Frith CD, Dolan RJ, Mazziotta JC. *Human Brain Function.* 1st ed. San Diego, CA: Academic Press; 1997:3–159.
6. *Diagnostic and Statistical Manual of Mental Disorders.* 4th ed. (DSM-IV). Washington, DC: American Psychiatric Association; 1994:123–163.
7. McKhann G, Drachman D, Folstein M, Katzman R, Price D, Stadlan EM. Clinical diagnosis of Alzheimer's disease: report of the NINCDS-ADRDA work group under the auspices of Department of Health and Human Services task force on Alzheimer's disease. *Neurology.* 1984;34:939–944.
8. Hughes CP, Berg L, Denziger WL, Coben LA, Martin RL. A new clinical scale for the staging of dementia. *Br J Psychiatry.* 1982;140:566–572.
9. Hodges JR. *Cognitive Assessment for Clinicians.* 1st ed. Oxford, England: Oxford Medical Publications; 1993:197–228.
10. Hodges JR, Patterson K. Is semantic memory consistently impaired early in the course of Alzheimer's disease? Neuroanatomical and diagnostic implications. *Neuropsychologia.* 1995;33:441–459.
11. Matsuda H, Yagishita A, Tsuji S, Hisada K. A quantitative approach to technetium-99m ethyl cysteinate dimer: a comparison with technetium-99m hexamethylpropylene amine oxime. *Eur J Nucl Med.* 1995;22:633–637.
12. Takeuchi R, Matsuda H, Yonekura Y, Sakahara H, Konishi J. Noninvasive quantitative measurements of regional cerebral blood flow using technetium-99m-L,L-ECD SPECT activated with acetazolamide: quantification analysis by equal-volume-split ^{99m}Tc-ECD consecutive SPECT method. *J Cereb Blood Flow Metab.* 1997;17:1020–1032.
13. Friberg L, Andersen AR, Lassen NA, Holm S, Dam M. Retention of ^{99m}Tc-bicisate in the human brain after intracarotid injection. *J Cereb Blood Flow Metab.* 1994;14(suppl 1):S19–S27.
14. Imon Y, Matsuda H, Ogawa M, Kogure D, Sunohara N. SPECT image analysis in Parkinson's disease subjects using statistical parametric mapping. *J Nucl Med.* 1999;40:1583–1589.
15. Talairach J, Tournoux P. *Co-Planar Stereotactic Atlas of the Human Brain.* 1st ed. Stuttgart, Germany: Thieme; 1988:37–110.
16. Friston KJ, Frith CD, Liddle PF, Frackowiak RSJ. Comparing functional (PET) images: the assessment of significant change. *J Cereb Blood Flow Metab.* 1991;11:690–699.
17. Friston KJ, Worsley KJ, Frackowiak RSJ, Mazziotta JC, Evans AC. Assessing the significance of focal activations using their spatial extent. *Hum Brain Mapping.* 1994;1:214–220.
18. Minoshima S, Foster NL, Kuhl DE. Posterior cingulate cortex in Alzheimer's disease. *Lancet.* 1994;344:895.
19. Minoshima S, Giordani B, Berent S, Frey KA, Foster NL, Kuhl DE. Metabolic reduction in the posterior cingulate cortex in very early Alzheimer's disease. *Ann Neurol.* 1997;42:85–94.
20. Ishii K, Sasaki M, Yamaji S, Kitagaki H, Mori E. Demonstration of decreased posterior cingulate perfusion in mild Alzheimer's disease by means of $H_2{}^{15}O$ positron emission tomography. *Eur J Nucl Med.* 1997;24:670–673.
21. Ibanez V, Pietrini P, Alexandar GE, et al. Regional glucose metabolic abnormalities are not the result of atrophy in Alzheimer's disease. *Neurology.* 1998;50:1585–1593.
22. Desgranges E, Baron J-C, Sayette V, et al. The neural substrates of memory systems impairment in Alzheimer's disease: a PET study of resting glucose utilization. *Brain.* 1998;121:611–631.
23. Fletcher PC, Frith CD, Grasby PM, Shallice T, Frackowiak RSJ, Dolan RJ. Brain systems for encoding and retrieval of auditory-verbal memory. *Brain.* 1995;118: 401–416.
24. Valenstein E, Bowers D, Verfaellie M, Heilman KM, Day A, Watson RT. Retrosplenial amnesia. *Brain.* 1987;110:1631–1646.
25. Rudge P, Warrington EK. Selective impairment of memory and visual perception in splenial tumours. *Brain.* 1991;114:349–360.
26. Minoshima S, Frey KA, Foster NL, Kuhl DE. Preserved pontine glucose metabolism in Alzheimer's disease: a reference region for functional brain image (PET) analysis. *J Comput Assist Tomogr.* 1995;19:541–547.
27. Braak H, Braak E. Neuropathological staging of Alzheimer-related changes. *Acta Neuropathol.* 1991;82:239–256.
28. Gomez-Isla T, Price TL, McKeel DW, Morris JC, Growdon JH, Hyman BT. Profound loss of layer II enthorhinal cortex neurons occurs in very mild Alzheimer's disease. *J Neurosci.* 1996;16:4491–4500.
29. Jack CR, Petersen RC, Xu YC, et al. Medial temporal atrophy on MRI in normal aging and very mild Alzheimer's disease. *Neurology.* 1997;49:786–794.
30. Bobinski M, Leon MJ, Convit A, et al. MRI of enthorhinal cortex in mild Alzheimer's disease. *Lancet.* 1999;353:38–40.
31. Ohnishi T, Hoshi H, Nagamachi S, et al. High-resolution SPECT to assess hippocampal perfusion in neuropsychiatric diseases. *J Nucl Med.* 1995;36:1163–1169.
32. Julin P, Lindqvist J, Svensson L, Slomka P, Wahlund LO. MRI-guided SPECT measurements of medial temporal lobe blood flow in Alzheimer's disease. *J Nucl Med.* 1997;38:914–919.
33. Rodriguez G, Nobili F, Copello F, et al. ^{99m}Tc-HMPAO regional cerebral blood flow and quantitative electroencephalography in Alzheimer's disease: a correlative study. *J Nucl Med.* 1999;40:522–529.
34. Kitayama N, Kogure D, Ohnishi T, et al. MRI-based volumetry of hippocampal gray-matter, and SPECT measurements of hippocampal blood flow for the diagnosis of Alzheimer's disease: comparison with statistical parametric mapping. *Brain Sci Ment Disord.* 1999;10:299–306.
35. Mori E, Yoneda Y, Yamashita H, Hirono N, Ikeda M, Yamadori A. Medial temporal structures relate to memory impairment in Alzheimer's disease: an MRI volumetric study. *J Neurol Neurosurg Psychiatry.* 1997;63:214–221.
36. Tohgi H, Takahashi S, Kato E, et al. Reduced size of right hippocampus in 39- to 80-year old normal subjects carrying the apolipoprotein E ε4 allele. *Neurosci Lett.* 1997;236:21–24.
37. Lehtovirta M, Kuikka J, Helisalmi S, et al. Longitudinal SPECT study in Alzheimer's disease: relation to apolipoprotein E polymorphism. *J Neurol Neurosurg Psychiatry.* 1998;64:742–746.
38. Haxby JV, Grady CL, Koss E, et al. Longitudinal study of cerebral metabolic asymmetries and associated neuropsychological patterns in early dementia of the Alzheimer type. *Arch Neurol.* 1990;47:753–760.
39. Smith GS, Leon ML, George AE, et al. Topography of cross-sectional and longitudinal glucose metabolic deficits in Alzheimer's disease: pathophysiologic implications. *Arch Neurol.* 1992;49:1142–1150.
40. Brown DRP, Hunter R, Wyper DJ, et al. Longitudinal changes in cognitive function and regional cerebral function in Alzheimer's disease: a SPECT blood flow study. *J Psychiatr Res.* 1996:30;109–126.